Entanglement of two harmonic modes coupled by angular momentum

L. Rebón and R. Rossignoli

Departamento de Física-Instituto de Física de La Plata, Universidad Nacional de La Plata,
C.C. 67, 1900 La Plata, Argentina

We examine the entanglement induced by an angular momentum coupling between two harmonic systems. The Hamiltonian corresponds to that of a charged particle in a uniform magnetic field in an anisotropic quadratic potential or, equivalently, to that of a particle in a rotating quadratic potential. We analyze both the vacuum and thermal entanglement, thereby obtaining analytic expressions for the entanglement entropy and negativity through the Gaussian state formalism. It is shown that vacuum entanglement diverges at the edges of the dynamically stable sectors, increasing with the angular momentum and saturating for strong fields, whereas at finite temperature entanglement is nonzero just within a finite field or frequency window and no longer diverges. Moreover, the limit temperature for entanglement is finite in the whole stable domain. The thermal behavior of the Gaussian quantum discord and its difference from the negativity is also discussed.

　　　　　　　　　　PACS number(s): 03.67.Mn, 03.65.Ud, 05.30.Jp

I. INTRODUCTION

The investigation of quantum entanglement and quantum correlations in distinct physical systems is of great interest for both quantum information and many-body physics [1–4]. While the evaluation of entanglement in systems with a high-dimensional Hilbert space is generally a difficult problem, boson systems described by quadratic Hamiltonians in the basic boson operators offer the invaluable advantage of admitting an exact evaluation of entanglement measures in both the ground and thermal states through the Gaussian state formalism [5–12]. The latter allows the entanglement entropy [13] and negativity [14,15] of any bipartition of a Gaussian state to be expressed in terms of the symplectic eigenvalues of covariance matrices of the basic operators. Moreover, the positive partial transpose separability criterion [16,17] is both necessary and sufficient for two-mode mixed Gaussian states [5] [as well as $(1, n − 1)$ bipartitions of n-mode Gaussian states [7]], turning the negativity into a rigorous entanglement indicator for these systems. There is presently a great interest in continuous-variable-based quantum information [18] where Gaussian states constitute the basic element.

In addition, an approximate yet analytic evaluation of the quantum discord [19,20] in two-mode Gaussian states was recently achieved [21,22] by restricting the local measurement that determines this quantity to a Gaussian measurement [18]. Quantum discord is a measure of quantum correlations that coincides with the entanglement entropy in pure states but differs essentially from entanglement in mixed states, where it can be nonzero even if the state is separable, i.e., with no entanglement. The current interest in quantum discord was triggered by its presence [23] in certain mixed-state-based quantum computation schemes that provide exponential speedup over classical ones [24] yet exhibit no entanglement [25]. Important properties of states with nonzero discord were recently unveiled [26–28].

The aim of this work is to examine, using the Gaussian state formalism, the entanglement and quantum correlations between two harmonic modes generated by an angular momentum coupling. Such a system arises, for instance, when considering a charged particle in a uniform magnetic field in an anisotropic quadratic potential or a particle in a rotating anisotropic harmonic trap [29–32]. The model has been employed in several areas, including the description of deformed rotating nuclei [31,32], anisotropic quantum dots in a magnetic field [33], and fast rotating Bose-Einstein condensates [34–37] in the lowest Landau level approximation [38–40]. Containing just quadratic couplings in the associated boson operators, the different terms in the Hamiltonian may also be simulated in principle by standard optical means [18,41]. For a general quadratic potential, the model exhibits a complex dynamical phase diagram [42], presenting distinct types of stable and unstable domains and admitting the possibility of stabilizing an initially unstable system by increasing the field or frequency [42]. The model provides an interesting and physically relevant scenario for analyzing the behavior of mode entanglement in different regimes and near the onset of different types of instabilities, with the advantage of allowing an exact analytic evaluation of entanglement and quantum correlation measures at both zero and finite temperatures. In addition, the present results indicate that mode entanglement can be easily controlled in this system by modifying the field or frequency, thus suggesting a potential for quantum information applications. The dynamics of entanglement in other two-mode systems was examined in Refs. [43–45].

In Sec. II we describe the model and derive the analytic expressions for the vacuum entanglement entropy and the thermal negativity. The basic features of quantum discord are also discussed. The detailed behavior of entanglement with the relevant control parameters is then analyzed in Sec. III, where we show that while vacuum entanglement diverges at the edges of stable sectors, being correlated with the angular momentum, at finite temperature entanglement is finite and nonzero just within a finite-field window and below a finite limit temperature. A comparison between the thermal behavior of the negativity and that of the Gaussian quantum discord is also made, which indicates a quite different thermal response of these two quantities, with the discord vanishing only asymptotically for $T \to \infty$. We summarize in Sec. IV.

II. FORMALISM

A. Model Hamiltonian

We consider a system described by the Hamiltonian

$$H = \tfrac{1}{2}\big(P_x^2 + k_x' Q_x^2\big) + \tfrac{1}{2}\big(P_y^2 + k_y' Q_y^2\big) - \omega(Q_x P_y - Q_y P_x), \tag{1}$$

which represents two harmonic modes coupled by an angular momentum term. Here Q_μ and P_μ stand for dimensionless coordinates and momenta ($[Q_\mu, P_\nu] = i\delta_{\mu\nu}$ and $[Q_\mu, Q_\nu] = [P_\mu, P_\nu] = 0$). Equation (1) arises, for instance, in the description of a particle of charge e and mass m in a general quadratic potential subject to a uniform magnetic field, parallel to a principal axis of the potential. Denoting this axis as z, such a Hamiltonian reads

$$\mathcal{H} = \frac{(\boldsymbol{P} - e\boldsymbol{A}/c)^2}{2m} + \frac{1}{2}\big(K_x \mathcal{Q}_x^2 + K_y \mathcal{Q}_y^2 + K_z \mathcal{Q}_z^2\big) \tag{2}$$

$$= \frac{1}{2}\left[\frac{\mathcal{P}_x^2 + \mathcal{P}_y^2}{m} + K_x' \mathcal{Q}_x^2 + K_y' \mathcal{Q}_y^2 - \Omega \mathcal{L}_z\right] + \mathcal{H}_z, \tag{3}$$

where $\boldsymbol{A} = \tfrac{1}{2}\boldsymbol{H} \times \boldsymbol{Q}$ is the vector potential, $\Omega = \frac{e|\boldsymbol{H}|}{mc}$ is the cyclotron frequency, $\mathcal{L}_z = \mathcal{Q}_x \mathcal{P}_y - \mathcal{Q}_y \mathcal{P}_x$, $\mathcal{H}_z = \frac{1}{2}(\frac{\mathcal{P}_z^2}{m} + K_z \mathcal{Q}_z^2)$, and $K_\mu' = K_\mu + m\Omega^2/4$. Equation (3) is also identical to the intrinsic Hamiltonian of a particle of mass m in a quadratic potential of constants K_μ' rotating around the z axis with frequency $\Omega/2$ [31,32].

The replacements $\mathcal{P}_\mu = P_\mu \sqrt{\hbar m \Omega_0}$ and $\mathcal{Q}_\mu = Q_\mu / \sqrt{m\Omega_0/\hbar}$ in Eq. (3), with Ω_0 a reference frequency, leads to $\mathcal{H} = \hbar\Omega_0 H + \mathcal{H}_z$, with H given by Eq. (1) and

$$k_\mu' = k_\mu + \omega^2, \quad k_\mu = \frac{K_\mu}{m\Omega_0^2}, \quad \omega = \frac{\Omega}{2\Omega_0}. \tag{4}$$

We note that in terms of the boson operators $b_\mu = (Q_\mu + iP_\mu)/\sqrt{2}$, the scaled angular momentum $L_z = \mathcal{L}_z/\hbar$ in Eq. (1) is

$$L_z = Q_x P_y - Q_y P_x = -i(b_x^\dagger b_y - b_y^\dagger b_x), \tag{5}$$

which can then be simulated by standard linear optics, although for such bosons the first two terms in Eq. (1) become

$\sum_{\mu=x,y} g_\mu^+(b_\mu^\dagger b_\mu + \tfrac{1}{2}) + g_\mu^-(b_\mu^2 + b_\mu^{\dagger\,2})$, with $g_\mu^\pm = \frac{k_\mu' \pm 1}{2}$, and require nonlinear means. If $K_x' > 0$, we can set $k_x' = 1$, i.e., $g_x^- = 0$, by adequately choosing Ω_0 in Eq. (4), but g_y^- remains nonzero in the relevant anisotropic case $k_y' \neq k_x'$, where $[H, L_z] \neq 0$. The change to normal x and y bosons, such that $H = \sum_{\mu=x,y} \sqrt{k_\mu'}(\tilde{b}_\mu^\dagger \tilde{b}_\mu + \tfrac{1}{2}) - \omega L_z$, will lead instead to an additional term proportional to $(1 - \sqrt{k_x'/k_y'})(\tilde{b}_x \tilde{b}_y - \tilde{b}_x^\dagger \tilde{b}_y^\dagger)$ in L_z.

B. Diagonalization and stability

If the parameter

$$\Delta = \sqrt{(k_x' - k_y')^2/4 + 2\omega^2(k_x' + k_y')} \tag{6}$$

is nonzero, the canonical transformation

$$P_\mu' = P_\mu + \gamma Q_{-\mu}, \quad Q_\mu' = \frac{Q_\mu - \eta P_{-\mu}}{1 + \eta\gamma}, \tag{7}$$

where $\gamma = \frac{2\Delta - k_x' + k_y'}{4\omega}$, $\eta = \frac{2\gamma}{k_x' + k_y'}$, and the labels (x,y) are now identified with $(+,-)$, allows Eq. (1) to be written as [42]

$$H = \sum_{\mu=\pm} \frac{1}{2}\big(\alpha_\mu P_\mu'^2 + \beta_\mu Q_\mu'^2\big), \tag{8}$$

where $\alpha_\pm = 1 - \frac{\omega}{\Delta}(\gamma \mp \omega)$ and $\beta_\pm = \frac{\Delta}{\omega}(\gamma \pm \omega)$. If $\Delta = 0$ and $\omega \neq 0$, a separable representation of the form of Eq. (8) in terms of canonical variables ($[Q_\mu', P_\nu'] = \delta_{\mu\nu}$ and $[P_\mu', P_\nu'] = [Q_\mu', Q_\nu'] = 0$) is not feasible. Such a possibility can arise in the repulsive case $k_\mu \leqslant 0$, when the 4×4 matrix representing the quadratic form in Eq. (1) is not diagonalizable with the symplectic metric and leads to nontrivial Jordan forms [42].

For general real values of k_μ' in Eq. (1), the coefficients α_μ and β_μ in Eq. (8) can be positive, zero, negative, and even complex [42]. We will consider here those cases for which Eq. (8) can be further written as

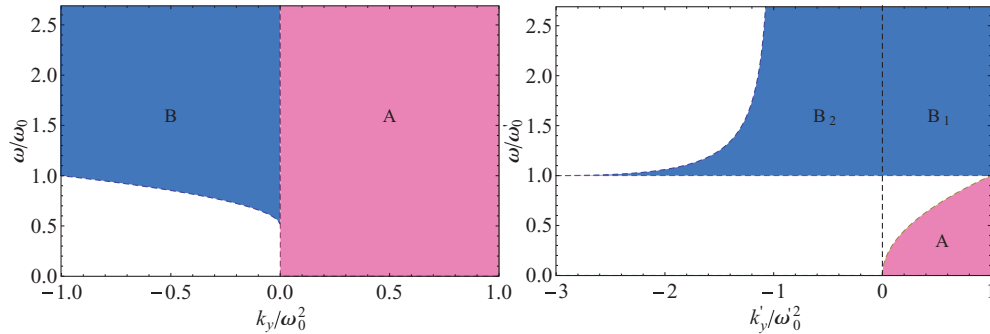$$H = \sum_{\mu=\pm} \lambda_\mu \left(b_\mu'^\dagger b_\mu' + \frac{1}{2}\right), \tag{9}$$

FIG. 1. (Color online) Left: Sectors with a discrete spectrum at fixed k_μ (particle in a magnetic field plus quadratic potential) in the anisotropy-frequency plane ($k_y/|k_x|, \omega/\omega_0$), where $\omega_0 = \sqrt{|k_x|}$. The positive-definite sector A corresponds to an attractive potential $k_\mu > 0$ for $\mu = x,y$, whereas the nonpositive sector B corresponds to a repulsive potential $k_\mu < 0$ for $\mu = x,y$ with $|\omega| > \omega_c$ [Eq. (11)]. Right: Same sectors at fixed $k_\mu' > 0$ (particle in a rotating quadratic potential) in the ($k_y'/k_x', \omega/\omega_0'$) plane, where $\omega_0' = \sqrt{k_x'}$ and we have set $k_x' > 0$. Here A is the positive-definite sector [Eq. (12)], B_1 is the nonpositive sector with $k_y' > 0$ [Eq. (13)], and B_2 is the nonpositive sector with $k_y' < 0$ [Eqs. (14) and (15)]. Quantities plotted in all figures are dimensionless.

$$|\lambda_\pm| = \sqrt{\alpha_\pm \beta_\pm} = \left(\frac{k'_x + k'_y}{2} + \omega^2 \pm \Delta\right)^{1/2}, \quad (10)$$

with λ_μ real and $b'_\mu = \sqrt{\beta_\mu/2\lambda_\mu}\, Q'_\mu + i\sqrt{\alpha_\mu/2\lambda_\mu}\, P'_\mu$ standard bosons ($[b'_\mu, b'^\dagger_\nu] = \delta_{\mu\nu}$ and $[b'_\mu, b'_\nu] = [b'^\dagger_\mu, b'^\dagger_\nu] = 0$) such that H exhibits a discrete spectrum. In these cases the matrix representing Eq. (1) is diagonalizable with the symplectic metric, with real symplectic eigenvalues [42].

At fixed k_μ in Eq. (4) (charged particle in a magnetic field), Eq. (9) is valid in the following domains [42] (Fig. 1):

(A) $k_x > 0$ and $k_y > 0$, where $\alpha_\pm > 0$, $\beta_\pm > 0$, and $\lambda_\pm > 0$. It is the standard case of an attractive quadratic potential, where H is positive definite and hence fully stable.

(B) $k_x < 0$, $k_y < 0$, and

$$|\omega| > \omega_c = \frac{\sqrt{-k_x} + \sqrt{-k_y}}{2}, \quad (11)$$

where $\alpha_+ > 0$ and $\beta_+ > 0$ but $\alpha_- < 0$ and $\beta_- < 0$, implying $\lambda_+ > 0$ but $\lambda_- < 0$ in Eq. (9). It is the case of a repulsive quadratic potential, where H becomes equivalent to a standard plus an inverted oscillator if $|\omega| > \omega_c$: It has no minimum energy, but is dynamically stable, as the motion remains bounded [42]. The dynamics around a quadratic potential maximum can then be stabilized by a sufficiently strong field.

(C) $k_x = k_y = 0$ and $\omega \neq 0$. It is the Landau case, where $\Delta = 2\omega^2$, $\alpha_+ = 1$, and $\beta_+ = 4\omega^2$, whereas $\alpha_- = \beta_- = 0$, leading to $\lambda_+ = 2|\omega|$ and $\lambda_- = 0$. Equation (9) becomes a standard plus a vanishing oscillator. Here the final choice of b'_- and $b'^\dagger_-$ is not fixed, as $\lambda_- = 0$. We will set $b'_- = \sqrt{\omega}\, Q'_- + i P'_-/\sqrt{4\omega}$, according to the $k_\mu \to 0$ limit of the isotropic case $k_x = k_y = k$, where $\lambda_\pm = \sqrt{k'} \pm \omega$, $\Delta = 2\omega\sqrt{k'}$, $\gamma = \sqrt{k'} = 1/\eta$, $\alpha_\mu = \frac{1}{2}\lambda_\mu/\sqrt{k'}$, $\beta_\mu = 2\lambda_\mu\sqrt{k'}$, and $k' = k + \omega^2$.

At fixed k'_μ in Eq. (1) (rotating potential), the previous sectors are seen quite differently. Sector (A) corresponds to $k'_x > 0$, $k'_y > 0$, and

$$|\omega| < \omega'_{c1} = \min[\sqrt{k'_x}, \sqrt{k'_y}], \quad (12)$$

indicating a maximum allowable frequency in an attractive rotating quadratic potential (right panel in Fig. 1). Sector (B) corresponds to

$$|\omega| > \omega'_{c2} = \max[\sqrt{k'_x}, \sqrt{k'_y}] \quad (13)$$

if $k'_x > 0$ and $k'_y > 0$. Thus, as the frequency $|\omega|$ is increased above ω'_{c1} a finite instability interval $\omega'_{c1} < |\omega| < \omega'_{c2}$ arises in the anisotropic case $k'_x \neq k'_y$, although dynamical stability is again recovered for $|\omega| > \omega'_{c2}$. In addition, sector (B) also corresponds here to $k'_x > 0$ and $k'_y < 0$ (or vice versa) provided [42]

$$|\omega| > \sqrt{k'_x}, \quad -k'_x \leqslant k'_y < 0, \quad (14)$$

$$\sqrt{k'_x} < |\omega| < \omega'_{c3} = \frac{k'_x - k'_y}{\sqrt{8(k'_x + k'_y)}}, \quad -3k'_x < k'_y < -k'_x. \quad (15)$$

Hence a quadratic potential repulsive in one of the axes can be stabilized by increasing the frequency above $\sqrt{k'_x}$ if $-3k'_x < k'_y < 0$, although stability holds just within a finite interval if

$-3k'_x < k'_y < -k'_x$. Finally, the Landau case (C) corresponds to $k'_x = k'_y = \omega^2$.

C. Covariance matrix

Both the vacuum $|0'\rangle$ of the primed bosons b'_μ in Eq. (9) and the thermal state

$$\rho = Z^{-1}\exp[-\beta H], \quad (16)$$

well defined in the stable region (A) [with $\beta = 1/T > 0$ and $Z = \mathrm{Tr}\exp(-\beta H) = \sum_{\mu=\pm}\{2\sinh(\beta\lambda_\mu/2)\}^{-1}$], are Gaussian states [5,7–12]. Any expectation value and in particular the entanglement between the x and y modes in these states will then be completely determined by the elements of the basic covariance matrix of the operators Q_μ and P_μ, which we define as [12] (note that here $\langle Q_\mu\rangle = \langle P_\mu\rangle = 0$)

$$\mathcal{D}^R = \langle RR^t\rangle - \mathcal{M}^R = \begin{pmatrix} Q & L \\ L^t & P \end{pmatrix} - \frac{1}{2}\mathcal{M}^R, \quad (17)$$

$$\mathcal{M}^R = RR^t - (RR^t)^t = i\begin{pmatrix} 0 & 1 \\ -1 & 0 \end{pmatrix}, \quad (18)$$

where $R = (Q_x, Q_y, P_x, P_y)^t$ and hence $Q_{\mu\nu} = \langle Q_\mu Q_\nu\rangle$, $P_{\mu\nu} = \langle P_\mu P_\nu\rangle$, and $L_{\mu\nu} = \langle Q_\mu P_\nu + P_\nu Q_\mu\rangle/2$.

Equation (17) is unitarily related to the non-negative bosonic contraction matrix [12,31]

$$\mathcal{D} = \langle ZZ^\dagger\rangle - \mathcal{M} = \begin{pmatrix} F & G \\ \bar{G} & 1 + \bar{F} \end{pmatrix}, \quad (19)$$

$$\mathcal{M} = ZZ^\dagger - [(Z^\dagger)^t Z^t]^t = \begin{pmatrix} 1 & 0 \\ 0 & -1 \end{pmatrix}, \quad (20)$$

where $Z = (b_x, b_y, b^\dagger_x, b^\dagger_y)^t$, $F_{\mu\nu} = \langle b^\dagger_\nu b_\mu\rangle$, $G_{\mu\nu} = \langle b_\mu b_\nu\rangle$, and $b_\mu = (Q_\mu + iP_\mu)/\sqrt{2}$. Since $R = \mathcal{U}Z$, with $\mathcal{U} = \binom{1\ 1}{-i\ i}/\sqrt{2}$, we have $\mathcal{D}^R = \mathcal{U}\mathcal{D}\mathcal{U}^\dagger$ and $\mathcal{M}^R = \mathcal{U}\mathcal{M}\mathcal{U}^\dagger$.

In both the vacuum and the thermal state [Eq. (16)] we have

$$\langle b'_\mu b'_\nu\rangle = 0, \quad \langle b'^\dagger_\mu b'_\nu\rangle = f'_\mu \delta_{\mu\nu}, \quad (21)$$

where $f'_\mu = 0$ in the vacuum state and

$$f'_\mu = -\frac{1}{\beta}\frac{\partial \ln Z}{\partial \lambda_\mu} - \frac{1}{2} = \frac{1}{e^{\beta\lambda_\mu} - 1} \quad (22)$$

in the thermal state. By inverting Eq. (7), we then obtain $\langle Q_x Q_y\rangle = \langle P_x P_y\rangle = L_{\mu\mu} = 0$ for $\mu = x, y$ and

$$\langle Q^2_\mu\rangle = \langle Q'^2_\mu\rangle + \frac{\eta^2}{(1 + \gamma\eta)^2}\langle P'^2_{-\mu}\rangle, \quad (23)$$

$$\langle P^2_\mu\rangle = \frac{1}{(1 + \gamma\eta)^2}\langle P'^2_\mu\rangle + \gamma^2\langle Q'^2_{-\mu}\rangle, \quad (24)$$

$$\langle Q_\mu P_{-\mu}\rangle = -\gamma\langle Q'^2_\mu\rangle + \frac{\eta}{(1 + \gamma\eta)^2}\langle P'^2_{-\mu}\rangle, \quad (25)$$

where

$$\langle Q'^2_\mu\rangle = \left(f'_\mu + \tfrac{1}{2}\right)\frac{\lambda_\mu}{\beta_\mu}, \quad \langle P'^2_\mu\rangle = \left(f'_\mu + \tfrac{1}{2}\right)\frac{\lambda_\mu}{\alpha_\mu}. \quad (26)$$

These averages provide all the elements of Eq. (17). The symplectic eigenvalues of $\mathcal{D}^R$ and $\mathcal{D}$ are coincident and given precisely by f'_μ and $-1 - f'_\mu$ [Eqs. (21) and (22)], with physical states corresponding to $f'_\mu \geqslant 0$.

They are just the standard eigenvalues of the matrix $\mathcal{DM} = \begin{pmatrix} F & -G \\ \bar{G} & -1-\bar{F} \end{pmatrix}$ or, equivalently, $\mathcal{D}^R\mathcal{M}^R = \mathcal{UDMU}^\dagger = i\begin{pmatrix} -L & Q \\ -P & L^t \end{pmatrix} - I/2$.

D. Vacuum entanglement

The entanglement of the vacuum $|0'\rangle$ is a measure of its deviation from a product state $|0_x\rangle \otimes |0_y\rangle$. It can be quantified through the entanglement entropy [13], which is just the von Neumann entropy of the reduced state $\rho_\mu = \mathrm{Tr}_{-\mu}\,\rho$ of any of the modes ($\mu = x,y$) since for a pure state ($\rho = |0'\rangle\langle0'|$) they are isospectral. The state ρ_μ is a Gaussian mixed state completely determined by the reduced 2×2 covariance matrix

$$\mathcal{D}_\mu^R = \begin{pmatrix} \langle Q_\mu^2 \rangle & L_{\mu\mu} \\ L_{\mu\mu} & \langle P_\mu^2 \rangle \end{pmatrix} - \tfrac{1}{2}\mathcal{M}^R, \tag{27}$$

whose symplectic eigenvalues are $f_\mu = \det^{1/2}[\mathcal{D}_\mu^R + \tfrac{1}{2}\mathcal{M}^R] - \tfrac{1}{2}$ and $-1 - f_\mu$. Here $L_{\mu\mu} = 0$ and hence

$$f_\mu = \sqrt{\langle Q_\mu^2 \rangle\langle P_\mu^2 \rangle} - \tfrac{1}{2}, \tag{28}$$

which is just the deviation of the mode uncertainty from its minimum value. The entropy of ρ_μ is therefore that of a boson system with average occupation f_μ:

$$S(\rho_\mu) = -\mathrm{Tr}\,\rho_\mu \log \rho_\mu = h(f_\mu), \tag{29}$$
$$h(f) = -f \log f + (1+f)\log(1+f), \tag{30}$$

which is just a positive concave increasing function of f_μ. The vacuum is then entangled if and only if $f_\mu > 0$, with $S \approx -f_\mu(\ln f_\mu - 1)$ for $f_\mu \to 0$ and $S \approx \ln f_\mu + 1$ for $f_\mu \to \infty$ [for base e logarithm in Eq. (30)].

In the vacuum case ($f_\mu' = 0$) Eqs. (23)–(28) lead to

$$f_\mu = \frac{1}{2}\left[\frac{\bar{\omega}}{\bar{\omega}_g}\left(\frac{\bar{\omega}_g^2 + \omega^2}{\bar{\omega}^2 + \omega^2}\right)^{1/2} - 1\right], \tag{31}$$

which is independent of μ, where

$$\bar{\omega} = \frac{\omega_x + \omega_y}{2}, \quad \bar{\omega}_g = \sqrt{\omega_x \omega_y} \tag{32}$$

denote the arithmetic and geometric averages of the original oscillator frequencies $\omega_\mu = \sqrt{k_\mu}$. Entanglement is thus completely determined by the ratios $\omega/\bar{\omega}$ and $\bar{\omega}_g/\bar{\omega}$ (with $\bar{\omega}_g/\bar{\omega} \leqslant 1$) or, equivalently, ω/ω_x and ω_y/ω_x. It is then nonzero for all $\omega > 0$ if $\omega_x \neq \omega_y$, i.e., $\bar{\omega} \neq \bar{\omega}_g$ (anisotropic case). In sector A, the ω_μ are positive, whereas in B they are both imaginary, implying

$$f_\mu = \frac{1}{2}\left[\frac{|\bar{\omega}|}{|\bar{\omega}_g|}\left(\frac{\omega^2 - |\bar{\omega}_g|^2}{\omega^2 - |\bar{\omega}|^2}\right)^{1/2} - 1\right], \quad k_\mu < 0. \tag{33}$$

E. Thermal entanglement

For a mixed bipartite state, such as the thermal state [Eq. (16)] at $T > 0$, entanglement is a measure of its deviation from a separable state [46], i.e., from a convex combination of product states $\rho_s = \sum_\alpha q_\alpha \rho_x^\alpha \otimes \rho_y^\alpha$, where $q_\alpha > 0$ and $\sum_\alpha q_\alpha = 1$. Such states can be created by local operations

and classical communication. For a two-mode Gaussian mixed state, entanglement can be quantified by the negativity [15], which is minus the sum of the negative eigenvalues of the partial transpose ρ^{t_y} of the total density matrix ρ, measuring then the degree of violation of the positive partial transpose criterion [16,17] by the entangled state. For a two-mode Gaussian state, a positive negativity is a necessary and sufficient condition for entanglement [5].

A partial transposition with respect to y implies the replacement $P_y \to -P_y$ in the full covariance matrix [Eq. (17)] [5,7–9], leading to a matrix $\tilde{\mathcal{D}}^R$. The negativity can then be evaluated in terms of the negative symplectic eigenvalues of this matrix, which will have eigenvalues $\tilde{f}_\mu$ and $-1 - \tilde{f}_\mu$, with $\tilde{f}_\mu \geqslant -1/2$ [12]. Replacing L_{xy} by $-L_{xy}$ in Eq. (17), we obtain here

$$\tilde{f}_\pm = (\tilde{\alpha} \pm \sqrt{\tilde{\alpha}^2 - \beta^2})^{1/2} - \tfrac{1}{2}$$
$$= \sqrt{\tfrac{1}{2}(\tilde{\alpha} + \beta)} \pm \sqrt{\tfrac{1}{2}(\tilde{\alpha} - \beta)} - \tfrac{1}{2}, \tag{34}$$

where $\tilde{\alpha}$ and β can be expressed in terms of the local symplectic eigenvalues f_μ [Eq. (28)] and the global symplectic eigenvalues f_μ' [Eq. (22)]:

$$\tilde{\alpha} = \tfrac{1}{2}(\langle Q_x^2 \rangle\langle P_x^2 \rangle + \langle Q_y^2 \rangle\langle P_y^2 \rangle) + \langle Q_x P_y \rangle\langle Q_y P_x \rangle$$
$$= \sum_\mu\left[\left(f_\mu + \tfrac{1}{2}\right)^2 - \tfrac{1}{2}\left(f_\mu' + \tfrac{1}{2}\right)^2\right], \tag{35}$$

$$\beta = \sqrt{(\langle Q_x P_y \rangle^2 - \langle Q_x^2 \rangle\langle P_y^2 \rangle)(\langle Q_y P_x \rangle^2 - \langle Q_y^2 \rangle\langle P_x^2 \rangle)}$$
$$= \prod_\mu\left(f_\mu' + \tfrac{1}{2}\right). \tag{36}$$

[Note that if $\tilde{\alpha}$ is replaced by $\alpha = \tfrac{1}{2}(\langle Q_x^2 \rangle\langle P_x^2 \rangle + \langle Q_y^2 \rangle\langle P_y^2 \rangle) - \langle Q_x P_y \rangle\langle Q_y P_x \rangle$, Eq. (34) becomes $f_\pm'$.] While f_μ depends on μ for $T > 0$, Eq. (35) depends just on the sum

$$\sum_\mu\left(f_\mu + \tfrac{1}{2}\right)^2 = \frac{\bar{\omega}^2(\omega^2 + \bar{\omega}_g^2)}{2\bar{\omega}_g^2(\omega^2 + \bar{\omega}^2)}\left(1 + 2\sum_\mu f_\mu'\right)$$
$$+ \frac{(\omega^2 - \bar{\omega}_g^2)(\omega^2 + 2\bar{\omega}^2) + 2\bar{\omega}^4}{2(\omega^2 + \bar{\omega}^2)(\omega^2 + \bar{\omega}^2 - \bar{\omega}_g^2)}\sum_\mu f_\mu'^2$$
$$+ \frac{\omega^2[(\omega^2 - \bar{\omega}_g^2)(2\bar{\omega}^2 - \bar{\omega}_g^2) + 2\bar{\omega}^4]}{\bar{\omega}_g^2(\omega^2 + \bar{\omega}^2)(\omega^2 + \bar{\omega}^2 - \bar{\omega}_g^2)}\prod_\mu f_\mu'.$$

The negativity can then be expressed as [12]

$$N = \frac{1}{2}(\mathrm{Tr}|\rho^{t_y}| - 1) = \frac{1}{2}\left[\prod_\mu \frac{1}{1 + \tilde{f}_\mu - |\tilde{f}_\mu|} - 1\right]$$
$$= \max\left[\frac{-\tilde{f}_-}{1 + 2\tilde{f}_-}, 0\right] \tag{37}$$

since only $\tilde{f}_-$ can be negative. The entanglement condition $\tilde{f}_- < 0$ leads to $\tilde{\alpha} > \tfrac{1}{8} + 2\beta^2$ or

$$\sum_\mu f_\mu(1 + f_\mu) > \sum_\mu f_\mu'(1 + f_\mu') + 2\prod_\mu f_\mu'(1 + f_\mu'), \tag{38}$$

which imposes a temperature-dependent lower bound on the average local occupation.

In the vacuum case $f'_\mu = 0$, Eq. (38) implies just $f_\mu > 0$, while Eqs. (34)–(37) reduce to

$$\tilde{f}_- = f_\mu - \sqrt{f_\mu(f_\mu + 1)}, \quad N = f_\mu + \sqrt{f_\mu(f_\mu + 1)},$$
$$(39)$$

with f_μ given by Eq. (31), in agreement with the general results for pure Gaussian states [12]. Both $-\tilde{f}_-$ and N are again concave increasing functions of f_μ at $T = 0$ and can be taken as alternative vacuum entanglement measures.

F. Quantum discord

Quantum discord [19] is essentially a measure of the deviation of a bipartite mixed quantum state from a classically correlated state, i.e., a state diagonal in a standard or conditional product basis. For a general bipartite system $A + B$, the quantum discord D^B can be defined as the minimum difference between the conditional von Neumann entropy of A after an unread local measurement M_B in B and the original quantum conditional entropy $S(A|B) = S(A,B) - S(B)$ [19]:

$$D^B = \min_{M_B} \sum_j p_j S(\rho_{A/j}) - [S(\rho_{AB}) - S(\rho_B)], \quad (40)$$

where, for a measurement M_B based on local projectors P_j ($\sum_j P_j = I_B$), $p_j = \mathrm{Tr}\rho_{AB} I_A \otimes P_j$ is the probability of outcome j and $\rho_{A/j}$ is the reduced state of A after such an outcome. Equation (40) can be also expressed as the minimum difference between the original mutual information $I(A : B) = S(A) - S(A|B)$, which measures all correlations between A and B, and that after the unread local measurement, $S(A) - \sum_j p_j S(\rho_{A/j})$, which contains the classical part of the quantum correlations [19,20].

For a pure state ($\rho^2_{AB} = \rho_{AB}$) both $S(\rho_{AB})$ and $S(\rho_{A/j})$ vanish and D^B reduces to the entanglement entropy $S(\rho_B) = S(\rho_A)$, with $D^A = D^B$ [19]. For a mixed state, however, D^B is not an entanglement measure, being in fact nonzero for most separable states [47] and vanishing just for those separable states of the form $\rho_c = \sum_j p_j \rho_{A/j} \otimes P_j$ (classically correlated with respect to B), which remain unaltered after the local measurement M_B. In general, $D^B \neq D^A$ for mixed states. Hence, for a bipartite system with a nondegenerate ground state in a thermal equilibrium state, such as the system under study, differences between quantum discord and entanglement and between D^A and D^B will arise only at finite temperature.

The exact evaluation of D^B involves a difficult minimization over all local measurements M_B. Nonetheless, for a two-mode Gaussian state, a minimization restricted to Gaussian measurements was recently shown to be analytically feasible [21,22,48]. For such measurements in the present system, Eq. (40) becomes, choosing $B = y$ and using Eqs. (22) and (29)–(30),

$$D^y = \min_{M_y} h(f_x^{M_y}) - [h(f'_+) + h(f'_-) - h(f_y)], \quad (41)$$

where $f_x^{M_y}$ denotes the symplectic eigenvalue of the covariance matrix $\mathcal{D}_x^{M_y}$ associated with $\rho_{x/j}$, which depends on the 2×2 covariance matrix $\mathcal{D}_{M_y}$ determining the local Gaussian

measurement M_y [21,22]. The final result was provided in Ref. [22] and can be fully expressed in terms of the local invariants $A = 4(f_x + \frac{1}{2})^2$, $B = 4(f_y + \frac{1}{2})^2$, $C = 2\sum_\mu(f'_\mu + \frac{1}{2})^2 - (f_\mu + \frac{1}{2})^2$, and $D = \prod_\mu 4(f'_\mu + \frac{1}{2})^2$, which determine the quantity $E_{\min}$ of Ref. [22], with $\min_{M_y} f_x^{M_y} = \frac{1}{2}\sqrt{E_{\min}} - \frac{1}{2}$. It can be shown that if $D^y > 1$ the two-mode Gaussian state is entangled [21,22]. Moreover, the only two-mode Gaussian states with $D^y = 0$ are product states [22]. The expression for D^x (local measurement in x) is obviously similar ($x \leftrightarrow y$ in previous formulas).

III. RESULTS

A. Vacuum entanglement

Let us now analyze the main features of Eq. (31). We first consider fixed k_μ in Eq. (4) (charged particle in a magnetic field). In the isotropic case $\omega_x = \omega_y$, $\bar{\omega} = \bar{\omega}_g$, and $f_\mu = 0$ $\forall \omega$. There is no entanglement since L_z commutes in this case with H and leaves the isotropic product vacuum invariant. For $|\omega_x - \omega_y| \ll \bar{\omega}$, Eq. (31) leads to

$$f_\mu \approx \frac{\omega^2}{16\bar{\omega}^2(\bar{\omega}^2 + \omega^2)}(\omega_x - \omega_y)^2 + O((\omega_x - \omega_y)^4), \quad (42)$$

indicating a quadratic vanishing of f_μ in this limit. Entanglement also vanishes for $\omega \to 0$ (no coupling), where

$$f_\mu \approx \frac{1}{4}\left(\frac{1}{\bar{\omega}_g^2} - \frac{1}{\bar{\omega}^2}\right)\omega^2 + O(\omega^4). \quad (43)$$

In contrast, for $\omega \to \infty$, a remarkable feature is that f_μ approaches a finite limit, which depends just on the anisotropy ω_y/ω_x: For $\omega \gg |\bar{\omega}|$ Eq. (31) leads to

$$f_\mu \approx \frac{1}{2}\left[\frac{\bar{\omega}}{\bar{\omega}_g} - 1\right] + O(\omega^{-2}). \quad (44)$$

In sector A, f_μ, and hence $S(\rho_\mu)$, is an increasing function of ω (Fig. 2). Mode entanglement is then enhanced just by increasing the field, although it will saturate for strong fields. This saturation is a consequence of the balance between the oscillator part and the coupling ωL_z in Eq. (1), as $k'_\mu = k_\mu + \omega^2$ also becomes large, thus reducing $\langle Q_\mu^2 \rangle$: For $\omega \to \infty$, $\langle Q_\mu^2 \rangle \approx \frac{\bar{\omega}}{2\omega_\mu}\omega^{-1} \to 0$ while $\langle P_\mu^2 \rangle \approx \frac{\bar{\omega}}{2\omega_{-\mu}}\omega \to \infty$, leading to the finite limit [Eq. (44)].

In contrast, f_μ, and hence entanglement, will diverge at the edges of the dynamically stable region. For instance, if $\omega_y \to 0$, $\bar{\omega} \to \omega_x/2$ whereas $\bar{\omega}_g \to 0$, implying $f_\mu \propto 1/\sqrt{\omega_y}$:

$$f_\mu \approx \frac{1}{2}\left[\left(\frac{\bar{\omega}}{2\omega_y}\right)^{1/2}\frac{\omega}{\sqrt{\bar{\omega}^2 + \omega^2}} - 1\right] \quad (45)$$

and hence $S(\rho_\mu) \approx \frac{1}{2}\log(\omega_x/\omega_y)$ plus constant terms. This divergence stems from that of $\langle Q_y^2 \rangle$ (or $\langle P_x^2 \rangle$) in this limit, with $\langle P_y^2 \rangle$ and $\langle Q_x^2 \rangle$ remaining constant [Eqs. (23)–(26)].

In the repulsive sector B, f_μ diverges for $\omega \to |\bar{\omega}| = \omega_c$ [Eq. (11)], where both $\langle Q_\mu^2 \rangle$ and $\langle P_\mu^2 \rangle$ diverge:

$$f_\mu \approx \frac{1}{2}\left[\left(\frac{|\bar{\omega}|}{\omega - |\bar{\omega}|}\right)^{1/2}\left(\frac{|\bar{\omega}|^2 - |\bar{\omega}_g|^2}{2|\bar{\omega}_g|^2}\right)^{1/2} - 1\right]. \quad (46)$$
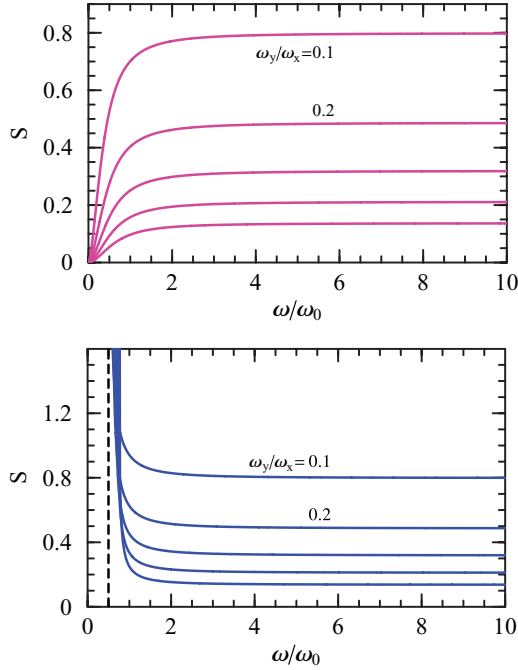
FIG. 2. (Color online) Entanglement entropy $S = S(\rho_\mu)$ [Eq. (29)] between the two modes as a function of ω in the vacuum of the Hamiltonian [Eq. (1)] at fixed $k_\mu = \omega_\mu^2$ for ratios $\omega_y/\omega_x = 0.1, \ldots, 0.5$ and $\omega_0 = |\omega_x|$. The top panel corresponds to sector A (attractive potential $k_\mu > 0$) and the bottom panel corresponds to sector B (repulsive potential $k_\mu < 0$ and $|\omega| > \omega_c$), where S diverges for $\omega \to \omega_c$ [Eq. (11)]. In both cases S approaches the same finite limit for $\omega \to \infty$.

It is then seen that here f_μ, and hence $S(\rho_\mu)$, decreases as ω increases from ω_c (Fig. 2, bottom panel), i.e., as the system becomes dynamically stabilized by the field, reaching, for $\omega \to \infty$, the same previous limit [Eq. (44)]. At fixed $|k_y/k_x|$, the vacuum entanglement is then strictly larger in the unstable sector B ($k_\mu < 0$).

At fixed k'_μ (rotating potential) the behavior with frequency is quite different (Fig. 3). We should now replace

$$\omega_\mu = \sqrt{\omega'^2_\mu - \omega^2}, \quad \omega'_\mu = \sqrt{k'_\mu} \quad (47)$$

in Eqs. (31) and (32). For $\omega'_x = \omega'_y$ there is of course no entanglement. For $|\omega'_x - \omega'_y| \ll \omega_x$, we have

$$f_\mu \approx \frac{\omega^2}{16(\omega^2 - \omega'^2_x)^2}(\omega'_x - \omega'_y)^2 + O((\omega'_x - \omega'_y)^4). \quad (48)$$

Entanglement also vanishes for $\omega \to 0$, where Eq. (43) still holds ($\omega'_\mu = \omega_\mu$ at $\omega = 0$).

Conversely, as ω increases, f_μ increases rapidly and, in contrast with the previous case, diverges for $\omega \to \omega'_{c1}$ [Eq. (12)], where, assuming $\omega'_{c1} = \omega'_y < \omega'_x$,

$$f_\mu \approx \frac{1}{2}\left[\left(\frac{\omega'^3_y(\omega'^2_x - \omega'^2_y)}{2(\omega'_y - \omega)(3\omega'^2_y + \omega'^2_x)^2}\right)^{1/4} - 1\right], \quad (49)$$

implying $S(\rho_\mu) \approx \frac{1}{4}\ln[\omega'_y/(\omega'_y - \omega)]$ plus constant terms. In this limit $\langle Q_y^2 \rangle$ and $\langle P_x^2 \rangle$ diverge while $\langle Q_x^2 \rangle$ and $\langle P_y^2 \rangle$ stay constant, as $\omega_y = \sqrt{\omega'^2_y - \omega^2} \to 0$. As ω increases further,
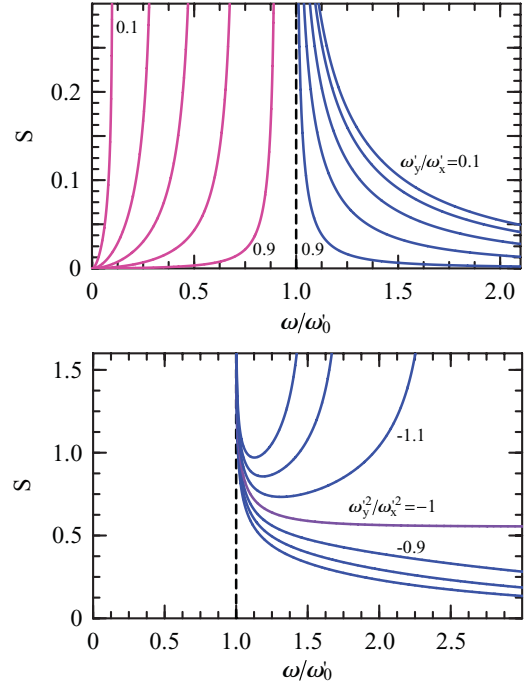

FIG. 3. (Color online) Entanglement entropy between the two modes as a function of ω in the vacuum of the Hamiltonian [Eq. (1)] at fixed $k'_\mu = \omega'^2_\mu$ for ratios $\omega'_y/\omega'_x = 0.1, 0.3, \ldots, 0.9$ (top) and $(\omega'_y/\omega'_x)^2 = -1.3, -1.2, \ldots, -0.7$ (bottom), with $\omega'_0 = \omega'_x$. The top panel corresponds to $k'_\mu > 0$, with the positive-definite sector A on the left, where S diverges for $\omega \to \omega'_{c1} = \omega'_y$, and the nonpositive sector B_1 on the right ($\omega > \omega'_{c2} = \omega'_x$), where S diverges at ω'_x and vanishes for $\omega \to \infty$. The bottom panel corresponds to $k'_x > 0$ and $k'_y < 0$ (sector B_2), where S diverges for $\omega \to \omega'_x$ and also $\omega \to \omega'_{c3}$ [Eq. (15)] if $(\omega'_y/\omega'_x)^2 < -1$. In the critical case $(\omega'_y/\omega'_x)^2 = -1$ ($k'_y = -k'_x$), f_μ and S saturate for large ω [Eq. (52)].

the system enters the instability window, although for $\omega > \omega'_{c2}$ [Eq. (13)], it recovers a discrete spectrum, entering sector B_1. For $\omega \to \omega'_{c2}$, f_μ diverges as in Eq. (49), with $\omega'_y \leftrightarrow \omega'_x$ if $\omega'_{c2} = \omega'_x$.

In sector B_1, f_μ, and hence the entanglement, decreases as ω increases, vanishing for $\omega \to \infty$, in contrast with the behavior at fixed k_μ in sector A. In this limit the vacuum of H now becomes that associated with ωL_z, which is an isotropic product Gaussian state with $L_z = 0$ and hence zero entanglement. Then $\langle Q_\mu^2 \rangle$ and $\langle P_\mu^2 \rangle$ stay finite and their product approaches minimum uncertainty, leading to

$$f_\mu \approx \frac{(\omega'^2_x - \omega'^2_y)^2}{32\omega^2(\omega'^2_x + \omega'^2_y)} + O(\omega^{-4}). \quad (50)$$

In the unstable domain B_2, the behavior with ω is the same as in B_1 when $k'_x > 0$ and $-k'_x < k'_y < 0$. However, for $k'_x > 0$ and $-3k'_x < k'_y < -k'_x$, we also have the upper instability limit in Eq. (15) (ω'_{c3}). In this case f_μ first decreases with increasing ω, reaching a minimum, but then starts again to increase, diverging for $\omega \to \omega'_{c3}$ where now both $\langle Q_\mu^2 \rangle$ and $\langle P_\mu^2 \rangle$ diverge, leading to

$$f_\mu \approx \frac{1}{2}\left[\left(\frac{\omega'_{c3}}{2(\omega'_{c3} - \omega)}\right)^{1/2} - 1\right]. \quad (51)$$
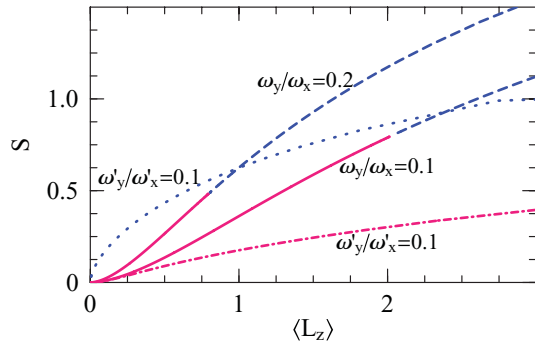
FIG. 4. (Color online) Entanglement entropy between the two modes as a function of the scaled average angular momentum $\langle L_z \rangle = \langle \mathcal{L}_z \rangle / \hbar$ [Eq. (5)] in the vacuum of Eq. (1) at fixed $k_\mu = \omega_\mu^2$ (solid and dashed lines) and at fixed $k'_\mu = \omega_\mu'^2$ (dash-dotted and dotted lines) for selected ratios ω_y / ω_x and ω'_y / ω'_x and variable ω. The solid and dash-dotted lines (red) correspond to sector A ($k_\mu > 0$ or $k'_\mu > 0$ and $|\omega| < \omega'_y$), the dashed and dotted lines (blue) correspond to sectors B ($k_\mu < 0$ and $|\omega| > \omega_c$) and B_1 ($k'_\mu > 0$ and $|\omega| > \omega'_x$). S is an increasing function of $|\langle L_z \rangle|$ in all sectors.

We then obtain different $O(\omega - \omega_c)^{-1/4}$ and $O(\omega_c - \omega)^{-1/2}$ divergences of f_μ at the stability borders ω'_x and ω'_{c3}, respectively.

In the special critical case $k'_y = -k'_x$ ($\omega'_y = i\omega'_x$), where $\omega'_{c3} \to \infty$, Eq. (31) leads to

$$f_\mu = \frac{1}{2}\left[\left(1 + \frac{\omega^2}{\sqrt{\omega^4 - \omega'^2_x}}\right)^{1/2} - 1 \right] \quad (52)$$

and hence to a finite asymptotic limit $f_\mu = \frac{1}{2}(\sqrt{2} - 1)$ for $\omega \to \infty$, in contrast with Eq. (50), as also appreciated in Fig. 3. In this limit $\langle Q_\mu^2 \rangle$ diverges whereas $\langle P_\mu^2 \rangle$ vanishes, the product approaching $1/2$. Hence, as ω increases, f_μ vanishes if $k'_y < -k'_x$, saturates if $k'_y = -k'_x$, and diverges (at $\omega = \omega'_{c3}$) if $-3k'_x < k'_y < -k'_x$.

The behavior of f_μ, and hence $S(\rho_\mu)$, with ω is qualitatively similar to that of the average angular momentum $\langle L_z \rangle$. At fixed k_μ, the latter also saturates for $\omega \to \infty$ [$\langle L_z \rangle \to (\bar{\omega}/\bar{\omega}_g)^2 - 1$] and diverges for $\omega \to \omega_c$ [$\langle L_z \rangle \propto (\omega - \omega_c)^{-1/2}$], whereas at fixed k'_μ it diverges for $\omega \to \omega'_{ci}$ [$\langle L_z \rangle \propto (\omega - \omega'_{ci})^{-1/2}$ for $i = 1,2$] and vanishes for $\omega \to \infty$. Entanglement is then an increasing function of $|\langle L_z \rangle|$ at fixed k_μ or k'_μ, as seen in Fig. 4, although it is not fully determined by $|\langle L_z \rangle|$, as the latter is not invariant under local transformations (in contrast with f_μ). At fixed $\langle L_z \rangle$, higher ratios $k_y / k_x < 1$ originate a higher entanglement (Fig. 4). For small ω, $\langle L_z \rangle \propto \omega$ and hence $f_\mu \propto \langle L_z \rangle^2$ for small $\langle L_z \rangle$ in sector A. However, at fixed k'_μ, $\langle L_z \rangle$ also vanishes for large ω, where $\langle L_z \rangle \propto \omega^{-3}$. Hence, in sector B_1 and according to Eq. (50), $f_\mu \propto \langle L_z \rangle^{2/3}$ for small $\langle L_z \rangle$, leading to an infinite initial slope (dotted line in Fig. 4). At fixed $\langle L_z \rangle$ and k'_μ, entanglement is then stronger in the unstable sector B_1 ($\omega > \omega'_{c2}$). An exceptional behavior occurs in the critical case $k'_y = -k'_x$ [Eq. (52)], where for $\omega \to \infty$, $\langle L_z \rangle \propto \omega^{-2}$ vanishes while f_μ remains finite. In this special limit there is finite entanglement with vanishing angular momentum. In contrast, close to the divergences, $f_\mu \propto \langle L_z \rangle$ ($\omega \to \omega_c$) or $\langle L_z \rangle^{1/2}$ ($\omega \to \omega'_{ci}$, $i = 1,2$), implying $S(\rho_\mu) \propto \ln \langle L_z \rangle$ for large $\langle L_z \rangle$.
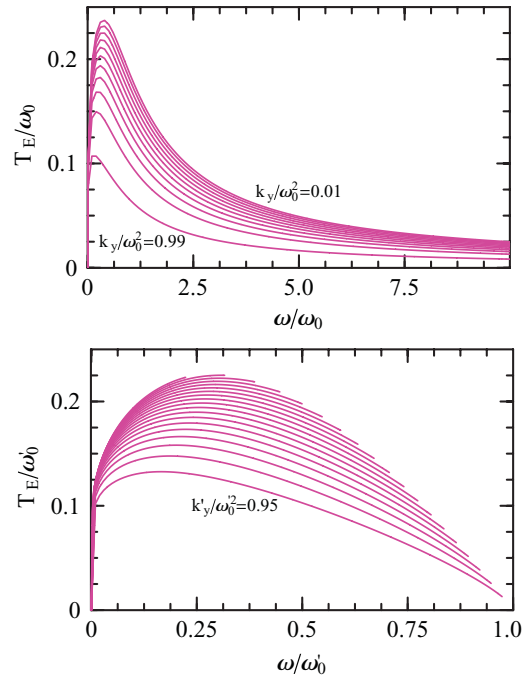

FIG. 5. (Color online) Scaled limit temperatures for entanglement T_E at fixed k_μ (top) and at fixed k'_μ (bottom), as a function of frequency for different ratios $k_y / k_x = 0.01, 0.1, \ldots, 0.9, 0.99$ (top) and $k'_y / k'_x = 0.05, 0.1, \ldots, 0.95$ (bottom), with $\omega_0 = \omega_x = \sqrt{k_x}$ and $\omega'_0 = \omega'_x = \sqrt{k'_x}$. At fixed k_μ, T_E vanishes for large ω [Eq. (55)] whereas at fixed k'_μ, it approaches a finite value at the upper stability limit $\omega'_{c1} = \sqrt{k'_y}$.

B. Thermal entanglement

Let us now examine the thermal entanglement in the stable sector A. We first depict in Fig. 5 the limit temperature for entanglement T_E, determined from the condition $\tilde{f}_- = 0$ [equality in Eq. (38)]. This temperature remains finite for all values of k_μ or k'_μ, including the edge of the sector ($k_\mu \to 0$ or $|\omega| \to \sqrt{k'_\mu}$), where the vacuum f_μ diverges. At the edge, $\lambda_- \to 0$ and hence a finite T already gives rise to a spread over all energy levels ($f'_- \to \infty$), which diminishes and eventually eliminates the entanglement. A related fundamental effect is that at finite $T > 0$, entanglement does not diverge at the edge, but stays finite or vanishes, depending on the value of T.

More precisely, for $\omega_y \to 0$ and fixed $\omega_x > 0$, $\lambda_+ \to \sqrt{4\omega^2 + \omega_x^2}$ whereas $\lambda_- \approx \omega_y \omega_x / \lambda_+$, implying $f'_- \approx T/\lambda_- \approx T\lambda_+ / \omega_x \omega_y$. Hence, in this limit Eqs. (34)–(36) lead to

$$\tilde{f}_- = \frac{1}{2}\left[\left(\frac{T\lambda_+^4 (1 + 2f'_+)^2}{\omega_x^2 [2\omega^2 \lambda_+ (1 + 2f'_+) + T\omega_x^2]} \right)^{1/2} - 1 \right], \quad (53)$$

which remains finite and above $-1/2$ if $T > 0$. This implies a finite negativity in this limit if $T > 0$, with $N \propto T^{-1/2}$ for $T \to 0$ according to Eq. (37). Therefore, at finite temperature the vacuum divergences of the entanglement can only be probed indirectly through the $T^{-1/2}$ behavior of N near the edge at sufficiently low T.

In addition, Eq. (53) entails a finite limit temperature T_E, obtained from the condition $\tilde{f}_- = 0$ in Eq. (53):

$$T_E = \frac{2(1 + 2f_+')\omega^2\omega_x^2\lambda_+}{(1 + 2f_+')^2\lambda_+^4 - \omega_x^4}, \quad (54)$$

which is a transcendental equation for T_E (f_+' depends on T_E). The maximum limit temperature T_E^M at fixed $k_x = \omega_x^2$ or $T_E'^M$ at fixed $k_x' = \omega_x'^2$ is in fact obtained in this limit ($\omega_y = 0$ or $\omega_y' = \omega$): At fixed k_x, $T_E^M \approx 0.24\omega_x$, attained at $\omega \approx 0.38\omega_x$, while at fixed k_x', $T_E'^M \approx 0.23\omega_x'$, attained at $\omega \approx 0.28\omega_x'$.

At fixed k_μ, the limit temperature T_E as a function of ω exhibits first a maximum and then vanishes for $\omega \to \infty$ (top panel in Fig. 5), i.e., in the limit where the vacuum entanglement saturates. The reason is that λ_- also vanishes for $\omega \to \infty$ ($\lambda_- \approx \omega_x\omega_y/2\omega$), implying $T_E \propto \omega^{-1}$ in this limit:

$$T_E \approx \frac{\omega_x\omega_y}{2\omega \ln\frac{\omega_x+\omega_y}{\omega_x-\omega_y}}. \quad (55)$$

In fact, for $\omega \to \infty$ and fixed k_μ (with $k_y < k_x$), Eqs. (34)–(36) lead to

$$\tilde{f}_- \approx \frac{1}{2}\left[\left(\frac{(1 + 2f_-')\omega_y}{\omega_x}\right)^{1/2} - 1\right], \quad (56)$$

such that $\tilde{f}_- = 0$ for $1 + 2f_-' = \omega_x/\omega_y$, which leads to Eq. (55). In contrast, for $\omega \to 0$, T vanishes logarithmically ($T_E \propto -1/\ln\omega$) and the same occurs for $\omega_y \to \omega_x$ since in these limits $\lambda_\pm$ remain both finite whereas the negativity vanishes. At fixed T, we then obtain a finite-frequency window for entanglement, which narrows for increasing temperature or decreasing anisotropy, as seen in Fig. 5 and also Fig. 6, where the negativity [Eq. (37)] is depicted. Entanglement ceases to be correlated with $\langle L_z \rangle$ as the temperature increases ($\langle L_z \rangle \propto \omega T$ for high T).

At fixed k_μ', the behavior of T_E and N look quite different, as now ω is bounded above by ω_y' (assuming $\omega_y' < \omega_x'$). For $\omega \to \omega_y'$, T_E is then determined by Eq. (54), with $\omega_x \to \sqrt{\omega_x'^2 - \omega^2}$, and remains finite. Actually, as verified in the bottom panel of Fig. 5, T_E acquires in this border its maximum value as ω increases at fixed k_μ' if $\omega_y' < \omega_{yc}' \approx 0.28\omega_x'$, while if $\omega_y' > \omega_{yc}'$ the maximum is attained at an intermediate frequency. Consequently, at fixed $T < T_E'^M$ there is again entanglement within a certain frequency window, which extends up to the stability border $\omega = \omega_y'$ if $\omega_y' < \omega_{yc}'$ or $T < T_E$ at $\omega = \omega_y'$ (bottom panel in Fig. 6). The absolute maximum $T_E'^M$ is obtained at this border precisely at $\omega_y' = \omega_{yc}'$. For $\omega \to 0$ or $\omega_y' \to \omega_x'$, T_E again decreases logarithmically.

C. Comparison with quantum discord

We finally compare in Fig. 7 the thermal behavior of the negativity with that of the Gaussian quantum discord D^y [Eq. (41)] and also D^x. For reference we have also plotted the entropy of one of the modes (x), no longer a measure of entanglement, just to indicate its coincidence with both D^y and D^x for $T \to 0$. While at $T = 0$ the negativity is just an increasing function of the entanglement entropy [Eqs. (29)–(39)], and hence of the quantum discord, the behavior for $T > 0$ is quite different. Although exhibiting a
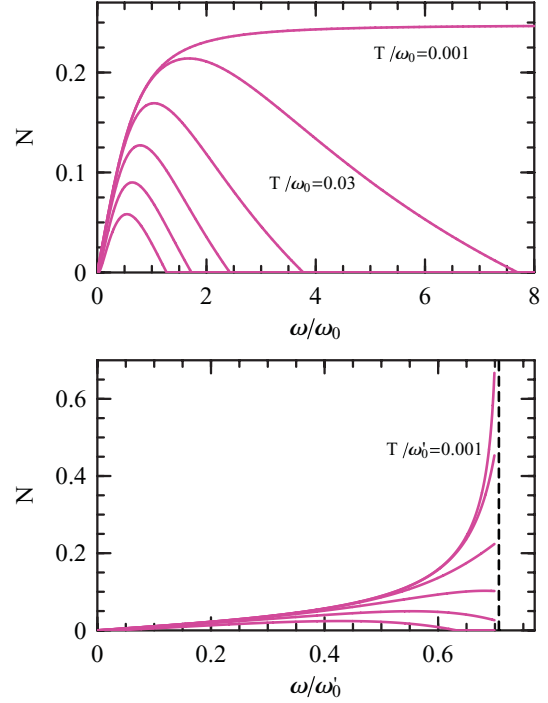

FIG. 6. (Color online) Negativity as a function of frequency at increasing temperatures $T/\omega_0 = 0.001, 0.03, 0.06, \dots, 0.15$, at fixed k_μ (top), for $k_y/k_x = 0.2$, and at fixed k_μ' (bottom), for $k_y'/k_x' = 0.5$. At $T > 0$, N is finite and nonzero just within a finite-frequency window.

similar initial decreasing trend [essentially due to the initial increase of the total entropy $S(\rho_{AB})$ in Eq. (40)], the Gaussian discord then starts to increase [due to the increase in the first term of Eq. (40)], vanishing only asymptotically for $T \to \infty$. Such a revival of the discord with increasing T was also observed in spin systems [49,50] and reflects the presence of quantum correlations in the excited eigenstates, which at these temperatures lead to a separable yet not classically correlated (in the sense of Sec. II F) thermal state. Since $D^\mu > 1$ implies entanglement [21,22], one can ensure here that $D^\mu < 1$ after the vanishing of the negativity ($T > T_E$), although this may not prevent D^μ from reaching a higher value than at $T = 0$ at some
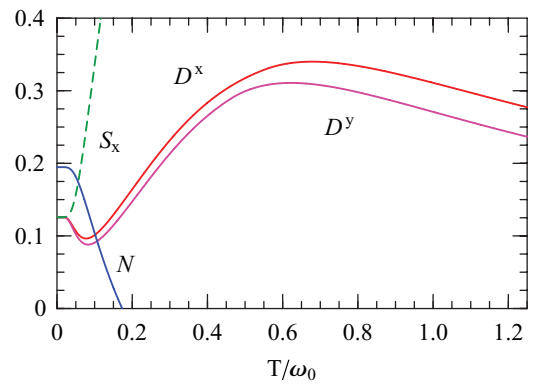

FIG. 7. (Color online) Negativity N, single-mode entropy $S_x = S(\rho_x)$, and the quantum discords D^y and D^x as a function of temperature for $\omega = \omega_0 = \sqrt{k_x}$ and $k_y = 0.2k_x$.

intermediate temperature, as seen in Fig. 7. For $T \to \infty$ we actually obtain, from Eq. (41) and the expression of Ref. [22], that $D^\mu \propto T^{-1}$:

$$D^y \approx \frac{\omega^2}{2T\sqrt{\omega^2 + \omega_x^2}}, \qquad (57)$$

with a similar expression for D^x after replacing ω_x by ω_y. Hence, for high T, D^μ becomes independent of ω_μ, with $D^x > D^y$ asymptotically if $\omega_y < \omega_x$, as verified in Fig. 7. We also note that the discord remains finite for $T > 0$ in the whole sector A.

IV. CONCLUSION

We have analyzed the entanglement induced by an angular momentum coupling of two harmonic modes. Full analytic expressions for the vacuum entanglement entropy and the thermal negativity were derived. The model exhibits a rich phase structure and admits distinct physical realizations (a particle in a magnetic field in an anisotropic harmonic trap or a particle in a rotating harmonic trap), which lead to different entanglement behaviors with the relevant control parameter. For instance, in sector A (stable vacuum), entanglement saturates for strong fields in the first case, but diverges at a finite frequency in the second case. Vacuum entanglement diverges at the onset of instabilities, being correlated with the average angular momentum and reaching higher values in unstable domains dynamically stabilized by the field or rotation. In contrast, thermal entanglement is finite and nonzero just below a finite limit temperature within a reduced-frequency window, diverging only for $T \to 0$ at the instability borders. We have also shown that after a short initial common trend, the thermal behavior of the Gaussian quantum discord becomes substantially different from that of entanglement, vanishing only asymptotically. It would be interesting to verify that a similar thermal behavior is also exhibited by other related measures of quantum correlations [48,51].

[1] M. A. Nielsen and I. L. Chuang, *Quantum Computation and Quantum Information* (Cambridge University Press, Cambridge, 2000).

[2] V. Vedral, *Introduction to Quantum Information Science* (Oxford University Press, Oxford, 2006).

[3] L. Amico, R. Fazio, A. Osterloh, and V. Vedral, Rev. Mod. Phys. **80**, 516 (2008).

[4] R. Horodecki, P. Horodecki, M. Horodecki, and K. Horodecki, Rev. Mod. Phys. **81**, 865 (2009).

[5] R. Simon, Phys. Rev. Lett. **84**, 2726 (2000).

[6] L. M. Duan, G. Giedke, J. I. Cirac, and P. Zoller, Phys. Rev. Lett. **84**, 2722 (2000).

[7] R. F. Werner and M. M. Wolf, Phys. Rev. Lett. **86**, 3658 (2001).

[8] K. Audenaert, J. Eisert, M. B. Plenio, and R. F. Werner, Phys. Rev. A **66**, 042327 (2002).

[9] G. Adesso, A. Serafini, and F. Illuminati, Phys. Rev. A **70**, 022318 (2004); A. Serafini, G. Adesso, and F. Illuminati, *ibid.* **71**, 032349 (2005).

[10] M. Cramer, J. Eisert, M. B. Plenio, and J. Dreißig, Phys. Rev. A **73**, 012309 (2006).

[11] G. Adesso and F. Illuminati, Phys. Rev. A **78**, 042310 (2008).

[12] J. M. Matera, R. Rossignoli, and N. Canosa, Phys. Rev. A **82**, 052332 (2010).

[13] C. H. Bennett, H. J. Bernstein, S. Popescu, and B. Schumacher, Phys. Rev. A **53**, 2046 (1996).

[14] K. Zyczkowski, P. Horodecki, A. Sanpera, and M. Lewenstein, Phys. Rev. A **58**, 883 (1998).

[15] G. Vidal and R. F. Werner, Phys. Rev. A **65**, 032314 (2002).

[16] A. Peres, Phys. Rev. Lett. **77**, 1413 (1996).

[17] M. Horodecki, P. Horodecki, and R. Horodecki, Phys. Lett. A **223**, 1 (1996).

[18] S. L. Braunstein and P. van Loock, Rev. Mod. Phys. **77**, 513 (2005).

[19] H. Ollivier and W. H. Zurek, Phys. Rev. Lett. **88**, 017901 (2001).

[20] L. Henderson and V. Vedral, J. Phys. A **34**, 6899 (2001).

[21] P. Giorda and M. G. A. Paris, Phys. Rev. Lett. **105**, 020503 (2010).

[22] G. Adesso and A. Datta, Phys. Rev. Lett. **105**, 030501 (2010).

[23] A. Datta, A. Shaji, and C. M. Caves, Phys. Rev. Lett. **100**, 050502 (2008).

[24] E. Knill and R. Laflamme, Phys. Rev. Lett. **81**, 5672 (1998).

[25] A. Datta, S. T. Flammia, and C. M. Caves, Phys. Rev. A **72**, 042316 (2005).

[26] D. Cavalcanti, L. Aolita, S. Boixo, K. Modi, M. Piani, and A. Winter, Phys. Rev. A **83**, 032324 (2011).

[27] A. Streltsov, H. Kampermann, and D. Bruß, Phys. Rev. Lett. **106**, 160401 (2011).

[28] M. Piani, S. Gharibian, G. Adesso, J. Calsamiglia, P. Horodecki, and A. Winter, Phys. Rev. Lett. **106**, 220403 (2011).

[29] J. G. Valatin, Proc. R. Soc. London **238**, 132 (1956).

[30] A. Feldman and A. H. Kahn, Phys. Rev. B **1**, 4584 (1970).

[31] P. Ring and P. Schuck, *The Nuclear Many-Body Problem* (Springer, New York, 1980).

[32] J. P. Blaizot and G. Ripka, *Quantum Theory of Finite Systems* (MIT Press, Cambridge, MA, 1986).

[33] A. V. Madhav and T. Chakraborty, Phys. Rev. B **49**, 8163 (1994).

[34] M. Linn, M. Niemeyer, and A. L. Fetter, Phys. Rev. A **64**, 023602 (2001).

[35] M. Ö. Oktel, Phys. Rev. A **69**, 023618 (2004).

[36] A. L. Fetter, Phys. Rev. A **75**, 013620 (2007).

[37] A. Aftalion, X. Blanc, and N. Lerner, Phys. Rev. A **79**, 011603(R) (2009).

[38] A. Aftalion, X. Blanc, and J. Dalibard, Phys. Rev. A **71**, 023611 (2005); S. Stock *et al.*, Laser Phys. Lett. **2**, 275 (2005).

[39] I. Bloch, J. Dalibard, and W. Zwerger, Rev. Mod. Phys. **80**, 885 (2008).

[40] A. L. Fetter, Rev. Mod. Phys. **81**, 647 (2009).

[41] J. Pěrina, Z. Hradil, and B. Jurčo, *Quantum Optics and Fundamentals of Physics* (Kluwer, Dordrecht, 1994); N. Korolkova, J. Pěrina, Opt. Commun. **136**, 135 (1996).

[42] R. Rossignoli and A. M. Kowalski, Phys. Rev. A **79**, 062103 (2009).

[43] A. P. Hines, R. H. McKenzie, and G. J. Milburn, Phys. Rev. A **67**, 013609 (2003).

[44] H. T. Ng and P. T. Leung, Phys. Rev. A **71**, 013601 (2005).

[45] A. V. Chizhov and R. G. Nazmitdinov, Phys. Rev. A **78**, 064302 (2008).

[46] R. F. Werner, Phys. Rev. A **40**, 4277 (1989).

[47] A. Ferraro, L. Aolita, D. Cavalcanti, F. M. Cucchietti, and A. Acin, Phys. Rev. A **81**, 052318 (2010).

[48] L. Mišta, R. Tatham, D. Girolami, N. Korolkova, and G. Adesso, Phys. Rev. A **83**, 042325 (2011).

[49] T. Werlang and G. Rigolin, Phys. Rev. A **81**, 044101 (2010).

[50] J. Maziero, H. C. Guzman, L. C. Celeri, M. S. Sarandy, and R. M. Serra, Phys. Rev. A **82**, 012106 (2010).

[51] R. Rossignoli, N. Canosa, and L. Ciliberti, Phys. Rev. A **82**, 052342 (2010).